Journal of Materials Chemistry A

RSC Publishing

PAPER

View Article Online
View Journal | View Issue

Cite this: J. Mater. Chem. A, 2013, 1, 3340

Transition-metal nitride nanoparticles embedded in N-doped reduced graphene oxide: superior synergistic electrocatalytic materials for the counter electrodes of dye-sensitized solar cells†

Xiaoying Zhang,‡[ab] Xiao Chen,‡[a] Kejun Zhang,[ab] Shuping Pang,[a] Xinhong Zhou,[c] Hongxia Xu,[a] Shanmu Dong,[a] Pengxian Han,[a] Zhongyi Zhang,[ab] Chuanjian Zhang[ab] and Guanglei Cui*[a]

Received 8th October 2012
Accepted 4th January 2013

DOI: 10.1039/c2ta00608a

www.rsc.org/MaterialsA

Transition-metal nitride TMN (MoN, TiN, VN) nanoparticle–N-doped reduced graphene oxide (NG) hybrid materials are presented as alternative low-cost platinum-free counter electrodes for dye-sensitized solar cells (DSCs). A high concentration of active catalytic sites and an efficient electronic/ionic mixed conducting network generated by the nanostructure afford promising synergistic effects on the electrocatalytic characteristics for triiodide reduction. On the basis of these advantages, these nanostructured hybrid based cells deliver significantly enhanced photovoltaic performances. The efficiencies of devices employing VN–NG, TiN–NG and MoN–NG are 6.279%, 7.498% and 7.913% respectively, which are comparable with that of Pt devices (7.858%). Such a design strategy is facile, cost effective and versatile, thus it may be extended to other inexpensive platinum-free counter electrode materials.

Introduction

Dye-sensitized solar cells (DSCs) have attracted much attention as potential candidates for the next generation of solar cells owing to their low cost, easy fabrication and respectable efficiency for the conversion of solar energy into electricity.[1–3] As an indispensable component of a DSC, the counter electrode (CE) is responsible for collecting electrons from the external circuit, transferring them back to the redox electrolyte and catalyzing the reduction of triiodide ions to iodide ions, making the cell a complete circuit.[4] In this regard, platinum (Pt) is the preferred material due to its superior conductivity and electrocatalytic activity.[5] However, its high cost and scarcity have restricted the large-scale application of DSCs. Consequently, it is still a key challenge to pursue an economical catalyst, endowed with both high catalytic activity and excellent electric conductivity.

In 1996, Kay and Grätzel first explored a graphite–carbon black mixture as a CE material and achieved a conversion efficiency of 6.7%.[6] Intensive research efforts have been stimulated to evaluate various carbonaceous materials. Multi-wall carbon nanotubes (MWCNTs),[7] single-wall carbon nanotubes (SWNTs),[8,9] mesoporous carbon,[10] carbon black,[11] and graphene[12] have also been proposed as alternative CEs in DSCs and have yielded conversion efficiencies of 7.7%, 4.5%, 6.18%, 9.1% and 6.81%, respectively. However, most of the corresponding cells suffered from unsatisfactory conversion efficiencies due to their low intrinsic electrocatalytic activities. Recently, conducting polymers such as poly(3,4-ethylenedioxythiophene) and polyaniline have also been employed as catalysts on FTO glasses for the CEs of DSCs.[13,14] However, the poor adhesion between conducting polymers and FTO glasses poses a long-term stability risk. More recently, several inorganic compounds have been introduced into DSCs as CE catalysts, such as metal nitrides,[15] carbides,[16] selenides[17] and sulfides.[18,19] In particular, group IVB–VIB transition-metal nitrides (TMNs) (*e.g.* MoN, TiN, VN, *etc.*) have attracted considerable attention, because of the coincidence of the electronic structure of TMNs with that of group VIII noble metals. The formation of TMNs modifies the nature of the d-band of the parent metal, resulting in a contraction of the metal d-band.[20] Such a d-band contraction results in a greater density of states (DOS) near the Fermi level in comparison with the parent metal. Consequently, for reactions involving the donation of electrons from catalysts, TMN

[a]The Qingdao Key Lab of solar energy utilization and energy storage technology, Qingdao Institute of Bioenergy and Bioprocess Technology, Chinese Academy of Sciences, Qingdao, 266101, P. R. China. E-mail: cuigl@qibebt.ac.cn

[b]Graduate School of the Chinese Academy of Sciences, Beijing, 100080, P. R. China

[c]Qingdao University of Science and Technology, Qingdao 266101, P. R.China

† Electronic supplementary information (ESI) available: SEM and TEM images of the bare MoN surface and *J–V* curves of various TiN based materials, cyclic voltammograms and EIS of different counter electrodes, equivalent circuit and the simulation data for EIS, elemental compositions of MoN–NG hybrids with different feed ratios. See DOI: 10.1039/c2ta00608a

‡ These authors contributed equally to this work.

catalysts might exhibit noble-metal-like electrocatalytic activity.[21] Nevertheless, the bothersome obstacle that exists in these nitride nanoparticles is their low electron transport efficiency, owing to abundant grain boundaries and defects.[22]

This limitation has encouraged tremendous effort to be applied to the modification of the nanostructure.[23–25] As a representative example, 1D carbon nanotubes (CNTs) have been employed as linkers to improve the electrical connection between TiN nanoparticles, owing to their excellent electrical conduction.[15] However, the efficiency was improved only slightly, probably because of the limited pathways for electron transfer, resulting in poor point contact between the TiN nanoparticles and columniform 1D CNTs (Scheme 1a). Nitrogen doped reduced graphene oxide (NG), an excellent 2D electronic conductor, may be favorable for the formation of a good contact area with nanoparticles endowing multiple pathways for electron transfer (Scheme 1b), since the nanoparticles could embed compactly onto the surface of its flakes *via* intermolecular forces (such as physisorption and electrostatic binding).[26,27] Moreover, this layered structure is supposed to ensure an extremely high surface/volume ratio, better electrode–electrolyte contact and fast diffusion of electrolyte species.

In this work, three kinds of hybrid CEs, with TMN (MoN, TiN, VN) catalyst nanoparticles anchored on the surface of NG layers, were prepared by a simple hydrothermal method *in situ*. Such hybrids are therefore reasonably expected to be interesting candidates for the further enhanced electrochemical performance of DSCs, integrating simultaneously both high electric conductivity and superior electrocatalytic activity synergetically.

Experimental

Herein, we developed a facile strategy to fabricate TMN (MoN, TiN, VN)–NG hybrids through a hydrolysis process combined with heat treatment at 800 °C under an ammonia atmosphere. The key to this strategy is to start with graphene oxide (GO) instead of graphene in the hydrolysis process, because the abundant oxygenated groups (likely hydroxyl and carbonyl groups) on the surface of GO could act as sites for metal nucleation through electrostatic forces.[28,29]

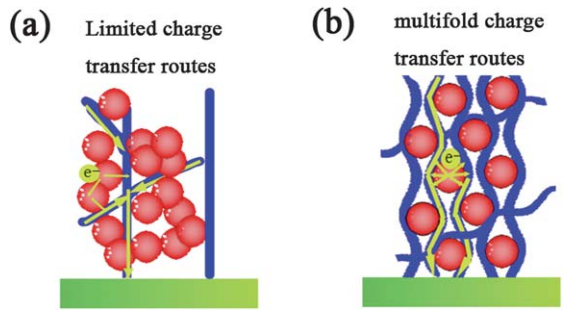

Scheme 1 Illustrative comparison between 1D CNTs (a) and 2D NG (b) nanostructured composite electrodes. For the 1D CNT composite, there are fewer connections between the spherical TMN and the columniform 1D nanomaterial, therefore, the electron transfer pathways are limited. However, for the 2D NG bridged electrode, TMN nanoparticles are enclosed by soft layers of NG as an electronic conductor, ensuring multiple charge transfer routes.

GO was prepared using graphite powder (Aldrich, powder, <20 micron, synthetic) according to a previous report by Hummers with minor revision.[30] In a typical procedure, molybdic acid served as the precursor and was dissolved in 50 mL of GO solution with ultrasonic treatment for about 2 h. Then 10 mL of dodecanethiol was added to the above solution while stirring for 10 min. The mixture was sealed in an autoclave and kept at 200 °C for 16 h. Then the precipitate was collected by centrifugation after the autoclave was cooled to room temperature. After washing with ethanol and deionized water, the solid product was dried at 70 °C for 24 h to obtain MoO_2–reduced graphene oxide (RGO). To prepare the MoN–NG hybrid material, the MoO_2–RGO was annealed at 800 °C under an NH_3 atmosphere. Here, the mole ratio of molybdic acid to GO was 3 : 7, and three other MoN–NG hybrids were also prepared and denoted *P* MoN–NG, where *P* is the molar percentage of molybdic acid.

Using the method discussed above, TiN–NG and VN–NG were also synthesized with different precursors. For a fair comparison, bare TMN nanoparticles and pristine NG were also prepared by the same procedure in the absence of GO or precursors.

The CE films were prepared on a precleaned fluorine-doped tin oxide (FTO) substrate by a doctor blade technique followed by drying at 110 °C. The thicknesses of these CEs were controlled to be about 7 μm. A mirror-like Pt/FTO electrode was obtained by electrodepositing a platinum layer on the surface of the FTO substrate, and its thickness was about 75 nm. A DSC with an active area of 0.16 cm^2 was constructed as described previously in the literature.[31] The liquid electrolyte was composed of 0.06 M LiI, 0.6 M 1,2-dimethyl-3-propylimidazolium iodide (DMPII), 0.03 M I_2, 0.5 M 4-*tert*-butylpyridine (TBP), and 0.1 M guanidinium thiocyanate with acetonitrile as the solvent.

Morphology information was obtained from field emission scanning electron microscopy (FESEM, HITACHI S-4800). X-ray diffraction (XRD) patterns were recorded with a Bruker-AXS Micro-diffractometer (D8 ADVANCE). Elemental analysis was performed using a Flash EA 1112 CHNS/O elemental analyzer from Thermo Scientific. The photocurrent–voltage characteristics of the DSCs were measured with a Newport (USA) solar simulator (300 W Xe source) and a Keithley 2420 source meter.

Cyclic voltammetry (CV) was carried out in a three-electrode system in an acetonitrile solution containing 0.1 M $LiClO_4$, 10 mM LiI, and 1 mM I_2. Pt foil served as a counter electrode and the non-aqueous Ag/Ag^+ couple was used as a reference electrode. Electrochemical impedance spectroscopy (EIS) measurements were performed using a Zahner Ennium electrochemical workstation by applying an AC voltage of 10 mV amplitude in the frequency range of 100 kHz to 100 mHz at room temperature. The fitting of the impedance spectra to the proposed equivalent circuit was performed using Zsimpwin software.

Results and discussion

It can be clearly observed from the SEM (Fig. 1a, c and e) and TEM (Fig. 1b, d and f) images of the TMN (MoN, TiN, VN)–NG

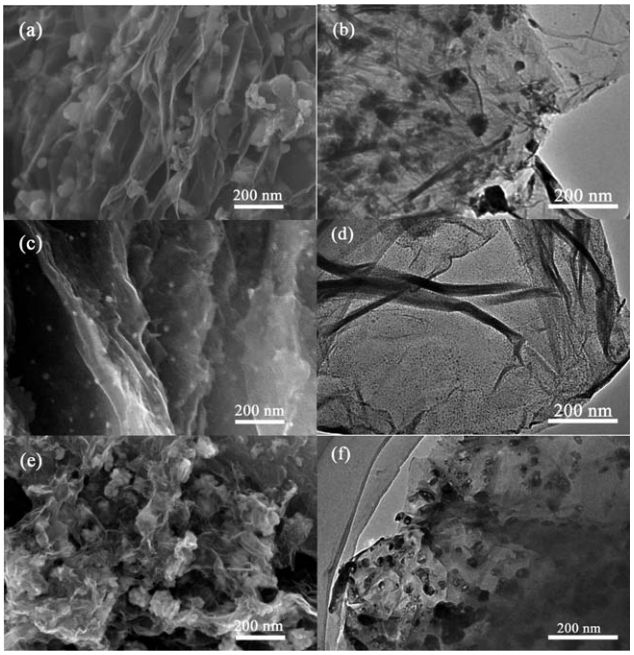

Fig. 1 Typical SEM images of MoN–NG (a), TiN–NG (c) and VN–NG (e). (b), (d) and (f) show their corresponding TEM images.

hybrids, that the graphene planar sheet-like structure is retained after the nitridation reaction and the TMN (MoN, TiN, VN) nanoparticles are inhomogeneously dispersed on the surface of the NG. Furthermore, it is also observed that the TMN nanoparticles are firmly anchored on the surface of the NG even after ultrasonication for SEM characterization. The compact combination is helpful for electron transfer between the TMN and the NG.

In contrast, large aggregated particles are observed for the bare MoN sample (Fig. S1, ESI†). These results verify that the presence of a layered structure is helpful in preventing the TMN (MoN, TiN, VN) nano-crystals from migrating and generating larger particles during the crystal formation process, which is consistent with a previous report.[28]

XRD patterns of TMN (MoN, TiN, VN), NG and TMN (MoN, TiN, VN)–NG hybrid materials are presented in Fig. 2. The as-synthesized NG displays a broad (002) diffraction peak at about 26° and a weak (100) diffraction peak at about 43° (Fig. 2), indicating the generation of a disordered stacked graphene nanosheet structure during the ammonia reduction of GO.[32] In the case of the hybrid materials, an additional small (002) diffraction peak at 26.5° can be assigned to NG. All the other diffraction peaks of the hybrid materials in Fig. 2a, b and c can be ascribed to the well-crystallized MoN structure (PDF#25-1367), TiN structure (PDF#65-0715) and VN structure (PDF#35-0768), respectively. These results indicate that the hybrids consist of disordered stacked NG and well-crystallized TMN (MoN, TiN, VN), which is consistent with previous reports.[33]

Fig. 3 illustrates the photocurrent density–voltage (*J–V*) curves of the DSCs fabricated with various CEs, and the corresponding photovoltaic parameters are summarized in Table 1. The devices using pristine nitride nanoparticles exhibit relatively inferior

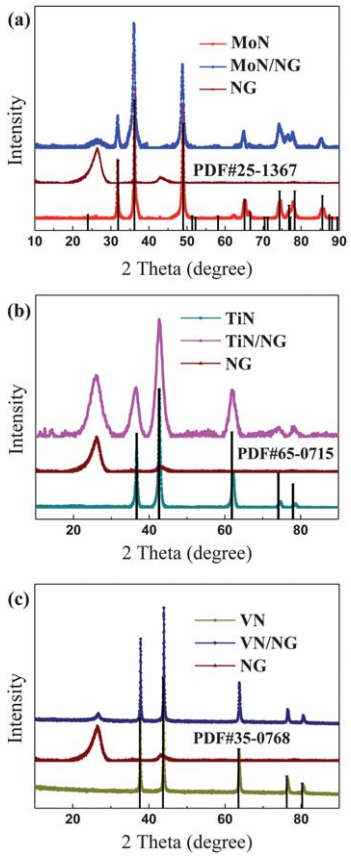

Fig. 2 XRD patterns of the MoN–NG (a), TiN–NG (b) and VN–NG (c) hybrids.

performances (2.463% for VN, 3.078% for TiN, and 6.179% for MoN), resulting from their low fill factors (FF) (28.75% for VN, 30.72% for TiN, and 58.98% for MoN). This is consistent with the results reported in the literature.[15,20,34] While in the case of pristine NG, the device also shows a low FF, which may be the result of poor adhesion of the NG sheets.[35] However, after integration of the above two kinds of material, the photovoltaic performance

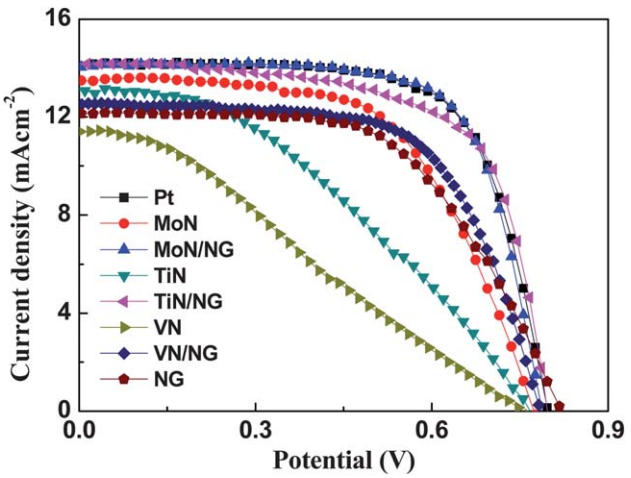

Fig. 3 Photocurrent–voltage (*J–V*) curves of the DSCs with different CEs consisting of nitride (MoN, TiN, VN) nanoparticles, pristine NG, (MoN, TiN, VN)–NG hybrids and Pt under 1 sun (AM 1.5) illumination.

Table 1 Photovoltaic parameters of the DSCs using different kinds of CE and simulated data from EIS spectra[a]

Samples	V_{OC} (V)	J_{SC} (mA cm^{-2})	FF (%)	η (%)	R_s (Ω cm^{-2})	R_{ct} (Ω cm^{-2})
Pt	0.796	14.22	69.39	7.858	23.70	6.557
MoN	0.774	13.54	58.98	6.179	24.88	6.563
MoN–NG	0.788	14.13	71.12	7.913	21.67	1.393
TiN	0.768	13.04	30.72	3.078	28.01	9.647
TiN–NG	0.796	14.16	66.52	7.498	25.16	2.211
VN	0.753	11.38	28.75	2.463	26.26	7.44
VN–NG	0.784	12.58	63.69	6.279	25.83	1.623
NG	0.821	12.14	58.21	5.800	22.57	8.177

[a] V_{OC}: open circuit voltage, J_{SC}: short circuit current density, FF: fill factor, η: energy conversion efficiency. R_s: series resistance and R_{ct}: charge-transfer resistance.

was significantly enhanced. Compared with the corresponding nitride, the FF was increased by 20% for MoN–NG, 120% for TiN–NG and 122% for VN–NG. In addition, the short-circuit current density (J_{SC}) and open-circuit voltage (V_{OC}) were improved slightly. Accordingly, the energy conversion efficiencies (η) are 7.913% and 7.498% for the MoN–NG and TiN–NG based devices, respectively, which are comparable to that of Pt–FTO devices (7.858%). Meanwhile, for the DSC with VN–NG, η is increased to 6.279%. Therefore, these hybrid CEs, integrating NG and nitride nanoparticles, yield better photovoltaic performances than either constituent could alone, *i.e.* the synergic effect is utilized (Fig. 2S, Fig. 3S and Table S1, ESI†).

Subsequently, the electrocatalytic activities of TMN (MoN, TiN, VN) nanoparticles, pristine NG, TMN (MoN, TiN, VN)–NG hybrids and Pt were evaluated by cyclic voltammetry (CV) under the same conditions (Fig. 4, see Fig. 4S, ESI,† for more details). For the Pt electrode, two pairs of redox peaks were observed, which is similar to the previous results in the literature.[36] The relatively negative pair is assigned to the redox reaction in (eqn (1)) and the positive pair is assigned to the redox reaction in (eqn (2)). In our case, the MoN–NG and TiN–NG hybrids both present two pairs of well-defined peaks with similar peak potentials to Pt, indicating excellent electrocatalytic characteristics, as for Pt. The improved current densities of the TMN (MoN, TiN, VN)–NG hybrid electrodes compared with their corresponding nitride nanoparticle based electrodes is partly ascribed to the more effective conductive network of NG forming bridges between nanoparticles. It is speculated that the above difference in the CV measurements directly influences the photovoltaic performance of the DSC as mentioned above.

$$I_3^- + 2e^- \rightleftharpoons 3I^- \quad (1)$$

$$3I_2 + 2e^- \rightleftharpoons 2I_3^- \quad (2)$$

In order to further elucidate the electrochemical properties of the as-prepared hybrid materials as CEs in DSCs, electrochemical impedance spectra (EIS) were recorded in a symmetric sandwich cell configuration consisting of two identical counter electrodes. The Nyquist plots are illustrated in Fig. 5 (the full range spectra are in Fig. 5S, ESI†). For the TMN (MoN, TiN, VN)–NG hybrids, three semicircles are visible, indicating that three kinetic stages are involved in the electrochemical process.[37] According to previous studies, the semicircle in the high frequency region corresponds to the charge-transfer resistance (R_{ct}) and capacitance of the CE–electrolyte interface, and the one in the middle frequency region is associated with the adsorption of iodine and triiodide on the electrode surface with a large active area.[38] The low-frequency semicircle is attributed to the Nernst diffusion impedance of the I^-/I_3^- redox species within a thin layer in the electrolyte, while the high frequency offset determines the series resistance (R_s).[38] Somewhat differently, the Nyquist plot of Pt exhibits two semicircles, since the adsorption process is not involved with the mirror-like Pt

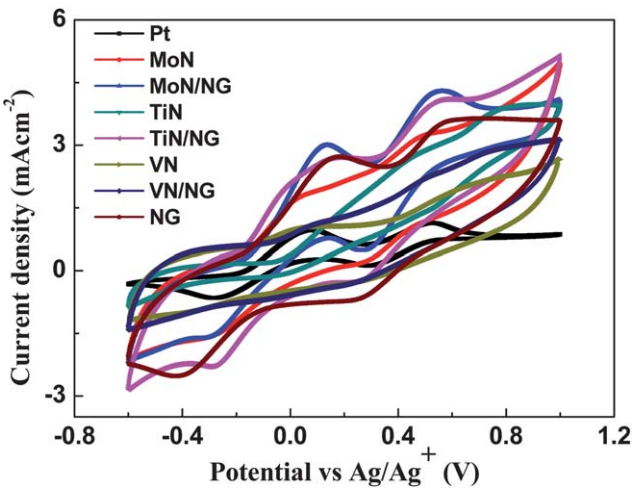

Fig. 4 Cyclic voltammograms of various CEs at a scan rate of 20 mV s^{-1} in 10 mM LiI, 1 mM I_2 acetonitrile solution containing 0.1 M $LiClO_4$ as the supporting electrolyte.

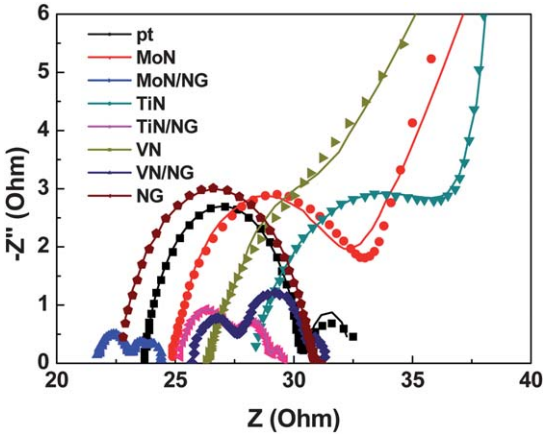

Fig. 5 Expanded range of impedance spectra of the symmetric cells with two identical CEs consisting of nitride (MoN, TiN, VN) nanoparticles, pristine NG, (MoN, TiN, VN)–NG hybrids and Pt over a measured frequency range of 100 kHz to 100 mHz. The symbols and lines correspond to the experimental and simulated data, respectively.

electrode.[39] Therefore different equivalent circuits were used to simulate the Nyquist plots (Fig. 6S, ESI†) and the simulated data from the EIS spectra are summarized in Table 1 and Table S2.†[39]

R_{ct} is an effective and widely used parameter for investigating the charge transfer process and thereby for evaluating the catalytic activity of a catalyst. The simulated R_{ct} values of the MoN–NG, VN–GNS and TiN–NG are 1.393 Ω cm^{-2}, 1.623 Ω cm^{-2} and 2.211 Ω cm^{-2}, respectively, much lower than that of the Pt electrode (6.557 Ω cm^{-2}), suggesting the superior electrocatalytic activity of the hybrid electrodes over the Pt–FTO electrode. The electrocatalytic activities of the TMN (MoN, TiN, VN)–NG hybrids are better than those of the corresponding pristine nitride material and the NG, which is a result of their lower R_{ct} (MoN has R_{ct} of 6.563 Ω cm^{-2}, VN of 7.44 Ω cm^{-2}, TiN of 9.647 Ω cm^{-2} and NG of 8.177 Ω cm^{-2}).

As a qualitative analysis, the semicircles in the low-frequency region for the hybrids are dramatically decreased in radius compared with those for the individual nitrides and the NG CEs. In addition, relative to the nitrides, the R_s of the hybrids declined as we expected. These results mean that the electron transfer resistance and the ion diffusion impedance were both reduced dramatically, which was a result of the excellent electrode–electrolyte contact and favourable electron transfer. As a result, it is expected that the FF of the hybrid CEs, which is related to the total impedance, could be remarkably improved and further ensure a promising performance.[40] This is corroborated by the photovoltaic performance of the DSC as mentioned above, clarifying that the bridged NG restricts the particle aggregation to generate more efficient interfacial active sites and leads to a significant synergic effect of the NG and the nitride nanoparticles.

Tafel polarization measurement is a powerful tool for the validation of the electrochemical characteristics of the TMN (MoN, TiN, VN)–NG hybrid electrodes. For a fair comparison, the nitride (MoN, TiN, VN) nanoparticles and pristine NG were also measured under the same conditions (Fig. 6). The anodic and cathodic branches of the logarithmic current density–potential (log J–U) plot show a larger slope for the TMN (MoN, TiN, VN)–NG hybrid CEs, indicating the presence of a larger exchange current density (J_0) in terms of the Tafel equation (eqn (3)). The obtained J_0 of these active materials have the following order: MoN–NG > VN–NG > TiN–NG > MoN > VN > NG > TiN. Furthermore, the tendency of R_{ct} to vary for different electrode materials as described by eqn (3) is corroborated by the results of the EIS.[41] Thus, the reaction activities for the cells also have the following order: MoN–NG > VN–NG > TiN–NG > MoN > VN > NG > TiN. After a comprehensive analysis of the EIS and Tafel polarization results, it can be concluded that the photovoltaic performance is in agreement with the EIS and Tafel polarization results on the whole.

$$J_0 = \frac{RT}{nFR_{ct}} \quad (3)$$

Where R_{ct} is extracted from the EIS, T is the temperature, R is the gas constant, and n is the total number of individual electrons.

As mentioned above, the TMN (MoN, TiN, VN)–NG hybrids are promising alternative CEs for the future large-scale fabrication of DSCs. In these hybrids, the superior electro-catalytic activity of nitride nanoparticles and the electron-transport network formed by NG each play an indispensable role in the high photovoltaic performance. An optimum balance between them should be obtained by optimizing the ratio of nitride to NG. Motivated by these considerations, three kinds of MoN–NG hybrids, *i.e.*, with different feed ratios (10% MoN–NG, 50% MoN–NG and 90% MoN–NG) were obtained and their photovoltaic performances were explored. Fig. 7 compares their performances under standard simulated AM 1.5 illumination at 100 mW cm^{-2} and detailed parameters are summarized in Table 2. It is obvious that with the increase in the molar percentage of MoN from 10% MoN–NG to 90% MoN–NG, J_{SC} increased sharply, while V_{OC} and FF changed slightly in the range 772 mV to 803 mV and 70.33% to 73.85%, respectively. Thus, η increases from 6.733% to 7.998%. The improvement in J_{sc} can be mainly ascribed to more efficient electrochemical catalytic sites on the MoN nanoparticles (Fig. 7S, ESI†). Otherwise, the relatively smooth change in FF reveals that the

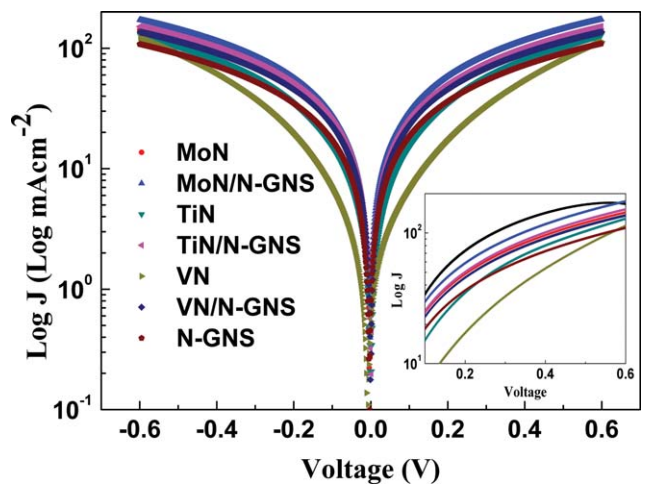

Fig. 6 Tafel polarization curves of symmetrical cells fabricated with two identical pristine NG electrodes, nitride electrodes, or hybrid electrodes. The inset shows an expansion of the *y*-axis in the voltage region 0 V to 0.6 V.

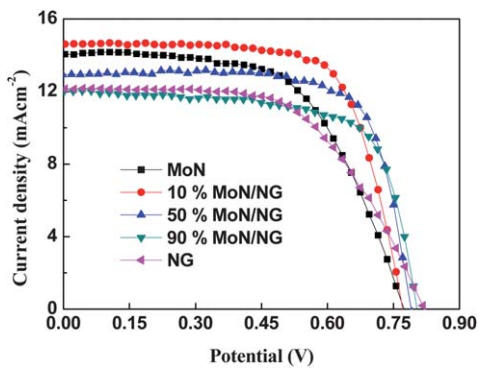

Fig. 7 Photocurrent–voltage (*J*–*V*) curves of the DSC based on MoN–NG with different feed ratios.

Table 2 Photovoltaic parameters of the DSC based on MoN–NG with different feed ratios

Samples	V_{oc} (V)	J_{sc} (mA cm^{-2})	FF (%)	η (%)
MoN	0.774	14.11	58.98	6.437
10% MoN–NG	0.772	14.62	70.87	7.998
50% MoN–NG	0.790	12.61	73.85	7.361
90% MoN–NG	0.803	11.92	70.33	6.733
NG	0.821	12.14	58.21	5.800

addition of about 10% of NG is enough for an efficient electronic/ionic mixed conducting network to be formed, leading to an excellent synergetic effect and a subsequent highly performing DSC. Furthermore, the loading amounts of MoN in the MoN–NG hybrids were determined by elemental analysis (Table 3S, ESI†). Ultimately, the highest conversion efficiency of 7.998% was achieved when the loading amount of MoN was 84.83%.

Conclusions

In summary, three kinds of hybrid were successfully fabricated by the hydrothermal method, in which TMN nanoparticles were highly dispersed on the surface of NG. Compared with individual TMN or NG, these as-prepared TMN (MoN, TiN, VN)–NG hybrid based cells delivered obviously improved photovoltaic performances. EIS measurements confirmed that the synergistic effect of TMN and NG on the electrocatalytic activity and ion diffusion was mainly responsible for the improvement of the electrochemical performance. The DSCs yielded efficiencies of 6.279%, 7.498% and 7.913% for VN–NG, TiN–NG and MoN–NG, respectively, which are much higher than that of a cells using a Pt CE. We believe that the current work paves the way for the fabrication of highly efficient and low-cost counter electrodes for DSCs.

Acknowledgements

We appreciate the support of the National Program on Key Basic Research Project of China (973 Program) (no. MOST2011CB935700), the "100 talents" program of the Chinese Academy of Sciences, the National Natural Science Foundation (grant no. 20901044, and 20902052), the Natural Science Foundation of Shandong Province (grant no. ZR2009BM014 BS2009NJ013).

Notes and references

1 A. Yella, H. W. Lee, H. N. Tsao, C. Yi, A. K. Chandiran, M. K. Nazeeruddin, E. W. Diau, C. Y. Yeh, S. M. Zakeeruddin and M. Gratzel, *Science*, 2011, **334**, 629–634.
2 M. Wang, N. Chamberland, L. Breau, J. E. Moser, R. Humphry-Baker, B. Marsan, S. M. Zakeeruddin and M. Gratzel, *Nat. Chem.*, 2010, **2**, 385–389.
3 B. Oregan and M. Gratzel, *Nature*, 1991, **353**, 737–740.
4 A. Hagfeldt and M. Gratzel, *Chem. Rev.*, 1995, **95**, 49–68.
5 Y. Zhao and L. Jiang, *Adv. Mater.*, 2009, **21**, 3621–3638.
6 A. Kay and M. Grätzel, *Sol. Energy Mater. Sol. Cells*, 1996, **44**, 99–117.
7 W. J. Lee, E. Ramasamy, D. Y. Lee and J. S. Song, *ACS Appl. Mater. Interfaces*, 2009, **1**, 1145–1149.
8 F. Bonaccorso, *Int. J. Photoenergy*, 2010, DOI: 10.1155/2010/727134.
9 K. Suzuki, M. Yamaguchi, M. Kumagai and S. Yanagida, *Chem. Lett.*, 2003, 28–29.
10 G. Q. Wang, W. Xing and S. P. Zhuo, *J. Power Sources*, 2009, **194**, 568–573.
11 T. N. Murakami, S. Ito, Q. Wang, M. K. Nazeeruddin, T. Bessho, I. Cesar, P. Liska, R. Humphry-Baker, P. Comte, P. Pechy and M. Gratzel, *J. Electrochem. Soc.*, 2006, **153**, A2255–A2261.
12 D. W. Zhang, X. D. Li, H. B. Li, S. Chen, Z. Sun, X. J. Yin and S. M. Huang, *Carbon*, 2011, **49**, 5382–5388.
13 J. B. Xia, N. Masaki, K. J. Jiang and S. Yanagida, *J. Mater. Chem.*, 2007, **17**, 2845–2850.
14 G. Wang, S. Zhuo and W. Xing, *Mater. Lett.*, 2012, **69**, 27–29.
15 G. R. Li, F. Wang, Q. W. Jiang, X. P. Gao and P. W. Shen, *Angew. Chem., Int. Ed.*, 2010, **49**, 3653–3656.
16 J. S. Jang, D. J. Ham, E. Ramasamy, J. Lee and J. S. Lee, *Chem. Commun.*, 2010, **46**, 8600–8602.
17 F. Gong, H. Wang, X. Xu, G. Zhou and Z. S. Wang, *J. Am. Chem. Soc.*, 2012, **134**, 10953–10958.
18 M. Wang, A. M. Anghel, B. Marsan, N. L. Cevey Ha, N. Pootrakulchote, S. M. Zakeeruddin and M. Gratzel, *J. Am. Chem. Soc.*, 2009, **131**, 15976–15977.
19 H. C. Sun, D. Qin, S. Q. Huang, X. Z. Guo, D. M. Li, Y. H. Luo and Q. B. Meng, *Energy Environ. Sci.*, 2011, **4**, 2630–2637.
20 M. Wu, X. Lin, Y. Wang, L. Wang, W. Guo, D. Qi, X. Peng, A. Hagfeldt, M. Gratzel and T. Ma, *J. Am. Chem. Soc.*, 2012, **134**, 3419–3428.
21 S. T. Oyama, *Catal. Today*, 1992, **15**, 179–200.
22 A. T. Bell, *Science*, 2003, **299**, 1688–1691.
23 E. Ramasamy, C. Jo, A. Anthonysamy, I. Jeong, J. K. Kim and J. Lee, *Chem. Mater.*, 2012, **24**, 1575–1582.
24 H. Xu, X. Zhang, C. Zhang, Z. Liu, X. Zhou, S. Pang, X. Chen, S. Dong, Z. Zhang, L. Zhang, P. Han, X. Wang and G. Cui, *ACS Appl. Mater. Interfaces*, 2012, **4**, 1087–1092.
25 X. Y. Zhang, X. Chen, S. M. Dong, Z. H. Liu, X. H. Zhou, J. H. Yao, S. P. Pang, H. X. Xu, Z. Y. Zhang, L. F. Li and G. L. Cui, *J. Mater. Chem.*, 2012, **22**, 6067–6071.
26 G. Williams, B. Seger and P. V. Kamat, *ACS Nano*, 2008, **2**, 1487–1491.
27 X. L. Li, H. L. Wang, J. T. Robinson, H. Sanchez, G. Diankov and H. J. Dai, *J. Am. Chem. Soc.*, 2009, **131**, 15939–15944.
28 L. S. Zhang, L. Y. Jiang, H. J. Yan, W. D. Wang, W. Wang, W. G. Song, Y. G. Guo and L. J. Wan, *J. Mater. Chem.*, 2010, **20**, 5462–5467.
29 R. Yu, L. Chen, Q. Liu, J. Lin, K.-L. Tan, S. C. Ng, H. S. O. Chan, G.-Q. Xu and T. S. A. Hor, *Chem. Mater.*, 1998, **10**, 718–722.

30 W. S. Hummers and R. E. Offeman, *J. Am. Chem. Soc.*, 1958, **80**, 1339.
31 C. J. Barbe, F. Arendse, P. Comte, M. Jirousek, F. Lenzmann, V. Shklover and M. Gratzel, *J. Am. Ceram. Soc.*, 1997, **80**, 3157–3171.
32 J. Shen, N. Li, M. Shi, Y. Hu and M. Ye, *J. Colloid Interface Sci.*, 2010, **348**, 377–383.
33 Z. Wen, S. Cui, H. Pu, S. Mao, K. Yu, X. Feng and J. Chen, *Adv. Mater.*, 2011, **23**, 5445–5450.
34 C. Shi, A. M. Zhu, X. F. Yang and C. T. Au, *Appl. Catal., A*, 2004, **276**, 223–230.
35 M.-Y. Yen, C.-K. Hsieh, C.-C. Teng, M.-C. Hsiao, P.-I. Liu, C.-C. M. Ma, M.-C. Tsai, C.-H. Tsai, Y.-R. Lin and T.-Y. Chou, *RSC Adv.*, 2012, **2**, 2725–2728.
36 A. I. Popov and D. H. Geske, *J. Am. Chem. Soc.*, 1958, **80**, 1340–1352.
37 Y. T. Tang, X. Pan, C. N. Zhang, S. Y. Dai, F. T. Kong, L. H. Hu and Y. F. Sui, *J. Phys. Chem. C*, 2010, **114**, 4160–4167.
38 F. Fabregat-Santiago, J. Bisquert, E. Palomares, L. Otero, D. B. Kuang, S. M. Zakeeruddin and M. Gratzel, *J. Phys. Chem. C*, 2007, **111**, 6550–6560.
39 J. D. Roy-Mayhew, D. J. Bozym, C. Punckt and I. A. Aksay, *ACS Nano*, 2010, **4**, 6203–6211.
40 N. Koide, A. Islam, Y. Chiba and L. Y. Han, *J. Photochem. Photobiol., A*, 2006, **182**, 296–305.
41 M. Wang, A. M. Anghel, B. t. Marsan, N.-L. Cevey Ha, N. Pootrakulchote, S. M. Zakeeruddin and M. Grätzel, *J. Am. Chem. Soc.*, 2009, **131**, 15976–15977.